International Journal for Multidisciplinary Research (IJFMR)
E-ISSN: 2582-2160 ● Website: www.ijfmr.com ● Email: editor@ijfmr.com

Treatment-Naïve Primary Osteosarcoma's Cellular and Molecular Heterogeneity is Revealed by Single-Cell RNA Sequencing in Canines

N. Ranga Sree[1], V. V. N. Sivanjaneyulu Gatte[2], Bellapukonda Indra Devi[3]

[1]Assistant Professor, Department of Computer Science and Engineering, Krishna University, Machilipatnam, Andhra Pradesh, India.
[2]Assistant Professor, Department of Mechanical Engineering, Krishna University, Machilipatnam, Andhra Pradesh, India
[3]Assistant Professor, Department of Computer Science and Engineering, Sri Vasavi Institute of Engineering and Technology, nandamuru, Pedana, Andhra Pradesh, India

ABSTRACT:
A diverse, aggressive bone cancer that disproportionately affects children and teenagers is called osteosarcoma (OS). The complicated tumor microenvironment (TME) of OS contributes to the paucity of therapeutic treatments. Therefore, in six treatment-naïve dogs with TME, we utilized single-cell RNA sequencing (scRNAseq) to characterize its cellular and molecular makeup. Primary OS that arises on its own. By examining 35,310 cells, we were able to characterize eight tumor-associated macrophage (TAM) populations, mature regulatory dendritic cells (mregDCs), and follicular helper T cells, among other 41 transcriptomically different cell types. According to cell-cell interaction study, TAMs and mregDCs are important players in the regulation of T cell-mediated immunity. Additionally, we discovered a high degree of similarity after completing a cross-species cell type gene signature homology study.

Keywords: RNA Sequencing

Introduction

Children and adolescents are disproportionately affected by osteosarcoma (OS), an aggressive bone cancer. Though the condition has a significant impact on the lives of those affected, there are currently no viable therapies available, and progress in developing combined surgical 1986 saw excision and adjuvant chemotherapy. A portion of the reason for the slow progress in developing OS treatments is the very uncommon occurrence that restricts patient enrollment in clinical trials. Large animal models have drawn more attention recently as a means of assessing and validating the promise of immunotherapeutics for a range of malignancies.Because dogs have a higher illness incidence, similar genetics and pathology, and are immunologically competent, spontaneously occurring canine OS is thought to be an ideal model of human OS. Dogs have, however, Malignant osteoblasts, osteoclasts, fibroblasts, macrophages, lymphocytes, and several other stromal and immunological components make up the

complex TME of osteosarcoma. When combined, the OS TME produces an environment that suppresses immunity, impeding antitumor immunological responses5. To better understand and target the biological components that support immune suppression, researchers have turned to the TME. Contrary to many other cancer types, findings in both humans and dogs indicate that an increase in macrophage abundance in OS lowers the rate of metastasis and improves survival. This surprising discovery emphasizes the need for a more thorough understanding of OS pathobiology, as do the unclear mechanisms of immune suppression in the OS TME.

Single-cell RNA sequencing, or scrRNA-seq, has become a useful technique for examining the transcriptomes of individual cells in heterogeneous tissues in recent years. The strategy gets beyond species-specific characteristics constraints by depending on an all-encompassing transcript capture technique that is only constrained by the accuracy of genome annotations. Significantly, the recently published human scRNA-seq landscapes of primary, recurrent, and metastatic OS provide as a benchmark for comparing cell type homology between canine and human OS. The current study's objectives were to assess human and canine cell type transcriptomic homologies and finish a molecular dissection of the canine OS TME using scRNA-seq.

Six primary osteosarcoma-affected dogs without prior therapy were included in the single-cell RNA sequencing reference dataset created for this investigation.There are 41 transcriptomically different cell types, according to our analysis. studied canine OS and demonstrated that the gene signatures for cell types in both canine and human OS are preserved. All things considered, the information produced here can help identify conserved OS TME characteristics and make it easier to investigate the canine osteosarcoma tumor microenvironment in more detail.

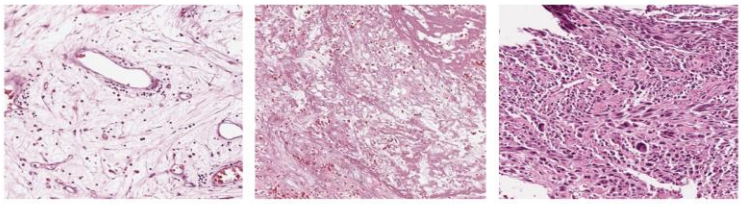

Figure 1: Sample Images from the dataset

Methods

Examine animals

Dogs in the trial were chosen based on the existence of a primary tumor in the appendix and the lack of prior treatment intervention. Every dog had radiographic evidence of OS, and the diagnosis was confirmed by a subsequent histological examination. The damaged limb of each research dog was amputated, and samples were gathered for single-cell RNA sequencing processing in less than 30 minutes. After that, the severed leg was delivered to the Colorado State University Veterinary Diagnostic Laboratory, where representative tumor samples were examined in order to validate the clinical diagnosis histopathologically. Based on pathology findings for each sample, the osteosarcoma subcategorization shown in Table 1 was verified by another veterinary pathologist. Every study received approval from Colorado State University (CSU).

Sample setup

The severed limb was cut down to the tumor's level using a stainless steel Three to five biopsy cores were taken from the tumor using a Michele trephine biopsy needle, which was used to target locations

with visible mass effects and/or cortical bone lysis. After that, phosphate was used to wash the biopsy cores. Buffered saline (PBS), chopped with a knife, and digested for 45 minutes at 37 °C with agitation using collagenase type II (250 U/mL) in Hanks' Balanced Salt Solution (HBSS) (Thermo Fisher Scientific Inc.). Samples were centrifuged for five minutes at 400 rcf after passing through a 70 µm cell strainer and being cleaned with PBS. Trypan blue exclusion was used to determine the presence of live cells in each of the individually obtained biopsies, and Thermo The mixed cell culture was placed onto a 3-mL Ficoll Paque (Cytiva; Marlborough, MA) and centrifuged for 30 minutes at 400 rcf with an acceleration of 9 and a brake of 0. This was done to enrich for live cells and eliminate debris. After density centrifugation, the layer interacting with the cell was collected, once more cleaned with PBS, and then allowed to resuspend for three to seven minutes at room temperature in a 10-mL Ammonium-Chloride-Potassium lysis buffer. A final wash was performed for 15 minutes at 100 rcf in order to get rid of platelets and tiny debris. Trypan blue exclusion was used to demonstrate that the cells had a viability more than 90%. The cells were then resuspended in 0.04% molecular grade BSA (Sigma-Aldrich; St. Louis, MO) in PBS and sent to a Chromium iX instrument (10x Genomics; Pleasanton, CA) for cell capture. Every sample was recorded.

Assembly and sequencing of libraries

Using a Chromium iX device, single cells were separated and molecular barcodes were applied with a goal of 5000 cells per sample. Two samples from each of the six dogs (dogs 1 and 2) were processed using a 5000-cell aim, with a combined goal of 10,000 cells for canines 1 and 2. Chromium Next GEM Single Cell 3′ v3.1 Kit and a standard Illumina library dual index library construction kit (10x Genomics) were used to process single cells. With a goal of 100,000 150 bp paired-end reads per cell, the sample quality was assessed using a LabChip (PerkinElmer; Waltham, MA) before being submitted for sequencing on an Illumina NovaSeq 6000 sequencer (Novogene Corporation; Sacramento, CA).

Examine the quantification and mapping

Reads were aligned to the canine genome, a count matrix was produced, and raw FASTQ sequencing data was processed using a Cell Ranger analytic pipeline (version 6.1.2, 10× Genomics). "Cell ranger count" was performed with the default parameters and aligned to a CanFam3.1 reference (Ensemble release 104) made in the manner previously mentioned21.

Integration and filtering of data

Using the Read10X() function, the count matrix for each sample was imported into R, and the CreateSeuratObject() function was used to transform it into a Seurat object18. Using PercentageFeatureSet() to count all reads mapped to features with the prefix "MT-," the percentage of reads mapping to mitochondrial chromosomes per cell ("percent.MT") was determined in order to estimate the number of dead/poor quality cells. Only cells that satisfied the following criteria were kept in each object: 200 < nFeature_RNA < 5500, percent.mt < 12.5, and 100 < nCount_RNA < 75000. The next step involved using DoubletFinder to locate and exclude potential cell doublets59. Seurat's alignment workflow48 was used to combine all of the samples into a single object after each sample had undergone quality control filtering and been normalized using SCTransform (Pearson residuals of regularized negative binomial regression). The steps in the alignment workflow were as follows: (1) determining which samples' variable characteristics were, (2) calculating the data for those features, (3)

pairwise integration of the data; (4) canonical correlation analysis (2000 integration anchors utilized) for the detection and filtering of conserved variable features (also known as "anchors") between samples. In order to reduce the effect of mitochondrial readings on dimension reduction and integration60, we employed the "percent.MT" value as a latent variable in a linear regression framework during the data scaling stage. After the data was integrated, the dataset was examined, and three low-quality clusters—which were distinguished by low UMI counts—were found and eliminated. After that, the filtered dataset was split up per sample into a list of count matrices and as the removal of cells may change the selection of variable features, Seurat's alignment method was repeated. The R program clustree61 was used to calculate the ideal clustering parameters (res = 0.8, dims = 45, n.neighbors = 40, min.dist = 0.35). After the completion of dimension reduction and visualization, two-dimensional, non-linear uniform manifold approximation and projection (UMAP) plots were used to project the data.

Analysis of subclustering

We subset the integrated dataset onto the population of interest for each major cell type in order to remove any extraneous cells. Following the division of the subset dataset into a list of count matrices by sample, the previously outlined Seurat alignment method was carried out. During the process of carrying out the integration of the reintegrated dataset, new variable features were found that can improve the capacity to identify uncommon cell types through unsupervised grouping. The following were the parameters for integration, dimension reduction, and clustering: tumor/stroma: min.dist = 0.5, n.neighbors = 50, dims = 40, res = 0.5, integration anchors = 3000, T cell: min.dist = 0.3, n.neighbors = 50, dims = 40, res = 0.6, integration anchors = 2500, Integration anchors for dendritic cells are 2000, res is 0.3, dims is 35, n.neighbors is 50, min.dist is 0.3, and integration anchors for macrophages and osteoclasts are 2500.

Classification of cells

Using gene set enrichment analysis, unsupervised clustering results, and manual annotation based on the literature for human cell type markers, high level cell type annotations were established. Essentially, characteristics such as CD3E/CD5/CD7 for T cells were employed to distinguish key cell types. The osteoclasts are represented by CTSK/ACP5/ATP6V0D2, the macrophages by CD68/AIF1/MRC1, the neutrophils by S100A12/CD4/CXCL8, the tumor/fibroblasts by COL1A1/ALPL/FAP, the dendritic cells by FLT3/CD1C/DNASE1L3, the endothelial cells by ESAM/PLVAP/CD34, the cycling cells by TOP2A/H1-5/MKI67, and the mast cells by FCER1A/GATA2/MS4A2. To support immune cell classifications, singleR and reference mapping to a canine leukocyte atlas were finished in addition to the use of canonical markers. Additional high-resolution identification of cells was finished using subclustering analysis on cells that belonged to each of the five primary cell populations: T cells, osteoclasts, dendritic cells, macrophage/monocyte, tumor/fibroblast, and so on. Supplementary Data 1 contains the cell type gene signatures that were found in this dataset using the FindAllMarkers() method (Wilcoxon Rank Sum test). Supplementary Data 2 and Supplementary contain curated short gene signatures for each cell type in addition to the complete gene signatures.

Visualization of features

Feature plots, dot plots, and violin plots were used to visualize the feature expression. The traits that were picked were based on previous biological understanding and classification of features with the

FindAllMarkers() function as statistically significant. For violin plots inside of a figure, the Y-axis scales are fixed. Normalized expressions for each feature on variable scales are displayed in feature plots. Gray/light purple coloration denotes low expression for all feature plots, while dark purple coloration denotes high expression. Scaled expression data is used in dot plots to show the variation in a gene's average value among the sampled cells.

Analysis of differential gene expression

Pseudobulk conversion was used to finish the differential gene expression (DGE) analysis, which was then processed using the DESeq2 pipeline64. Low abundance features—defined as features with fewer than 10 raw counts—were used before DESeq2. were eliminated from all tested cells. Statistically significant features were those with an adjusted P-value of less than 0.05 (calculated using the Benjamini and Hochberg correction method) and a log2 (fold change) larger than 0.5865.

Analysis of gene set enrichment

When the gene lists produced by DGE analysis were subjected to follow-up gene set enrichment analysis (GSEA), the significantly upregulated and Features that were downregulated were handled differently. The clusterProfiler and msigdbr R packages were utilized to evaluate the upregulated and downregulated gene lists and infer pathway activity. Terms that, after applying the Benjamin and Hochberg correction procedure, with an adjusted P value of 0.05 or below were considered significantly enriched. We completed GSEA on cell type clusters using the R package singleseqgset in addition to applying GSEA after DGE analysis. A competitive gene set enrichment test, based on a Correlation Adjusted Mean RAnk gene set test68, was employed in the analysis. The mean and log2 (fold change) To perform GSEA, the expression for each feature within each cell type was computed. False discovery rate (FDR) was used to adjust P values for multiple comparisons. The resulting corrected P values were then filtered to keep only terms where the value of at least one cell type was less than 0.05. A heatmap was used to illustrate the top pathways (weighted by P value) after the enrichment values had been scaled.

Analysis of copy number variation

CopyKAT was used to perform copy number variation (CNV) analysis on cells containing more than 2000 unique molecular identities (UMIs)14. To put it briefly, the method divided the human genome into variable genomic bins of 220 kb each in order to create a genome-wide copy number profile at a resolution of roughly 5 Mb for every single cell. When determining the CNV status, each Eash sample was analyzed separately using a known normal cell population made up of osteoclasts, neutrophils, macrophages, and T cells. After being taken out of the CopyKat output files and added to the integrated dataset, the CNV status was shown in the UMAP space for each individual cell classification. This method was limited to determining if a cell was diploid or aneuploid. We did not assess individual chromosomal alterations because of incompatibility. We also used the infer CNV algorithm on the dataset as a supplement to the Copy KAT analysis, and the results were comparable in terms of the aneuploid and diploid classifications15. In short, an ordered gene file created with the Ensembl CanFam3.1.104 gene transfer tool was used to execute the infer CNV method. format (.gtf) file that served as the foundation for the single-cell data alignment reference. The canine gene locations were then used to generate an infercnv object, and endothelial cells and macrophages were chosen as the

"normal" reference populations. After that, Infer CNV was used with the default parameters and the suggested "cutoff" option set to 0.1.

Activity of regulators

The Single-Cell Regulatory Network Inference and Clustering (pySCENIC) Python implementation was utilized to deduce the activities of cell types' gene regulatory networks. In order to conclude this study, the function convert_orthologs() from the orthogene R package71 was used to convert the gene symbols from canine to human. Genes with duplicate mappings in the canine or human annotations were removed from the matrix and not included in the subsequent analysis during the conversion process. After loading the count matrices containing the transformed gene symbols into SCANPY, a normal pySCENIC procedure was carried out using the default settings. The regulatory feather files utilized in the analysis were named hg38__refseq-r80__10kb_up_and_down_tss.mc9nr.feather and were downloaded from https://resources.aertslab.org/cistarget/. hg38__ refseq-r80__tss.mc9nr.feather, 500 bps up and 100 bps down. Regulon specificity scores (rss) were computed using AUCell following the prediction of regulon activity with pySCENIC. The rss values were then utilized to infer regulon activity in the cell types examined.

Analysis of inference for cell-cell interactions

Cell-cell interactions within the tumor microenvironment were inferred using the R package CellChat35. With a list of recognized Using human receptor-ligand pairings obtained from CellChat, we computed the intensity and weight of the interaction scores, which indicate the likelihood of two cells interacting. The final completely annotated dataset containing 41 cell types was used for initial analysis, and a subset of just immune cells (excluding the four main cell types—fibroblast, endothelium, osteoblast, and cycling osteoblast) were used for secondary analysis. As mentioned in the "Regulon activity" section, the raw count matrices were removed before analysis, and the gene symbols were changed from canine to human. In general, the research assessed how ligand-expressing cells—also known as senders or outgoing signals—interacted with receptor-expressing cells. Based on the law of mass action and the average expression values of receptors and ligands within cell types, conclusions on possible interactivity were then drawn. Permutation testing was utilized to ascertain the statistical enrichment of interaction networks, and an adjusted P value < 0.05 was employed to establish importance. After identifying the enriched cell-cell interaction networks, we used the reported receptor and ligand expression patterns to further classify each enriched pathway as "immune specific," "immune related," and "non-immune" The process of categorizing a subset of interaction networks (PD-L1, CD80, and CD86) as immune regulatory was part of the analysis of the immune cell subset.

Analysis of human OS homology

Six human OS samples without any treatment were acquired using the NCBI GEO database accession GSE16245412. The count matrices that were provided by the The six dog OS tumor samples from earlier studies were preprocessed using the same settings, and those objects were put into the filter as Seurat objects. Low resolution unsupervised clustering was used to annotate the human dataset, with reference to the original publication, in an effort to replicate the original annotations. The raw count matrices from each dataset were retrieved, and canine gene symbols were translated from canine to human as mentioned in the "Regulon activity" section, before data integration between species took

place. After gene symbols were converted, the 12 OS samples—six canine and six human—were combined into a single object using the The Seurat alignment process remained the same, as previously said, but 3000 variable features were chosen as anchors. Then, using the hclust() function and technique, hierarchical clustering was finished using SCTransform normalized counts. "Complete" is selected. FindAllMarkers() was used to create subsequent cell type gene signatures, and the corresponding dataset's DGE analysis was used to contrast the different cell types within each species. A Jaccard similarity index was computed using the resulting cell type gene signatures, and scatter plots were produced using the signed P values, which were given a sign (+/−) based on the log2 (fold change).

Statistics and reproducibility

Raw data from a total of 8 canine scRNA-seq osteosarcoma samples were generated in this study. Two of the 8 samples were technical replicates, which were considered as one sample when completing computational analysis to retain a total of 6 biological replicates. Biological replicates were used for pseudobulk differential gene expression analysis, while cellular replicates were used for all other analysis completed in this study. Detailed descriptions of the statistical analyses and significance thresholds used in this study are provided in the respective methods section.

Reporting summary

Further information on research design is available in the Nature Portfolio Reporting Summary linked to this article.

Data availability

Raw sequencing data are available on the NCBI Gene Expression Omnibus database under the accession number GSE252470. The annotated dataset is availablefor browsing at the UCSC Cell Browser (https://cells.ucsc.edu/?ds= canine-os-atlas) 74, and the processed data (Seurat v4.3.0 RDS objects) are available on Zenodo (https://doi.org/10.5281/zenodo.10666968) 75. Results of all differential gene expression analysis and cell type gene signatures are provided in Supplementary Data files.

References

1. Lindsey, Brock A., Justin E. Markel, and Eugenie S. Kleinerman.” Osteosarcoma overview.” Rheumatology and therapy 4.1(2017):25-43.
2. Song, Q., Merajver, S.D., Li, J.Z.: Cancer classification in the genomics era: ve contemporary problems. Human Genomics 9 (2015).
3. Idikio, H.A.: Human cancer classification: A systems biology-based model integrating morphology, cancer stem cells, proteomics, and genomics.Journal of Cancer 2 (2011).
4. S. Wang, D. M. Yang, R. Rong, X. Zhan, G. Xiao, Pathology image analysis using segmentation deep learning algorithms, The American journal of pathology 189 (2019)1686-1698.
5. P. Picci, Osteosarcoma (osteogenic sarcoma), Orphanet journal of rare diseases 2 (2007) 6.
6. H.-C. Shin, H. R. Roth, M. Gao, L. Lu, Z. Xu, I. Nogues, J. Yao, D. Mollura, R. M. Summers, Deep convolutional neural networks for computer-aided detection: Cnn architectures, dataset characteristics and transfer learning, IEEE transactions on medical imaging 35 (2016) 1285-1298.
7. W. Rawat, Z. Wang, Deep convolutional neural networks for image classi_cation: A comprehensive review, Neural computation 29 (2017) 2352-2449.

8. S. Wang, D. M. Yang, R. Rong, X. Zhan, G. Xiao, Pathology image analysis usingsegmentation deep learning algorithms, The American journal of pathology 189 (2019) 1686-1698.
9. A. Serag, A. Ion-Margineanu, H. Qureshi, R. McMillan, M.-J. Saint Martin, J. Diamond,P. O'Reilly, P. Hamilton, Translational ai and deep learning in diagnostic pathology, Frontiers in Medicine 6 (2019).
10. F. Chollet, et al., Keras, https://github.com/fchollet/keras, 2015.
11. Shin, H.C.; Roth, H.R.; Gao, M.; Lu, L.; Xu, Z.; Nogues, I.; Yao, J.; Mollura, D.; Summers, R.M. Deep convolutional neural networks for computer-aided detection: Cnn architectures, dataset characteristics and transfer learning. IEEE Trans. Med. Imaging **2016**, 35, 1285–1298. [CrossRef].
12. Deng, J.; Dong, W.; Socher, R.; Li, L.J.; Kai, L.; Li, F.-F. Imagenet: A large-scale hierarchical image database. In Proceedings of the 2009 IEEE Conference on Computer Vision and Pattern Recognition, Miami, FL, USA, 20–25 June 2009; pp. 248–255.
13. Krizhevsky, A.; Sutskever, I.; Hinton, G.E. Imagenet classification with deep convolutional neural networks. Commun. ACM **2017**,60, 84–90. [CrossRef].

14. ejbahAhammad, Mohammad Joynul Abedin, Md. Asiqur Rahman Khan, Md. Abdul Alim,Mohammad Abu Tareq Rony, K.M. RashedulAlam, D. S. A. Aashiqur Reza, Iktear Uddin, "A Proficient Approach to Detect OsteosarcomaThrough Deep Learning" 2022 10th IEEE International Conference on Emerging Trends inEngineering Technology Signal and Information Processing(ICETET-SIP-22)
15. D M Anisuzzamana, HoseinBarzekar, Ling Tong, Jake Luo, Zeyun Yu, "A Deep Learning Study on Osteosarcoma Detection fromHistological Images"arXiv:2011.01177v1 [eess.IV] 2 Nov 2020.
16. Ioannis A. Vezakis, George I. Lambrouand George K. Matsopoulos , "Deep Learning Approaches to Osteosarcoma Diagnosis andClassification: A Comparative Methodological Approach"Cancers2023, 15, 2290. https://doi.org/10.3390/cancers15082290.
17. SushoptiGawade, Ashok Bhansali, Kshitij Patil, Danish Shaikh, "Application of the convolutional neural networks and supervised deep-learning methods for osteosarcoma bone cancer detection" Healthcare Analytics 3 (2023) 100153.https://doi.org/10.1016/j.health.2023.100153.
18. M. D'Acunto, M. Martinelli, and D. Moroni, "Deep Learning Approach to Human Osteosarcoma Cell Detection and Classification," Cryptology and Network Security Lecture Notes in Computer Science, pp. 353–361, Jan. 2018.
19. Huang, Bingsheng, et al. "Feasibility of multi-parametric magnetic resonance imaging combined with machine learning in the assessment of necrosis of osteosarcoma after neoadjuvant chemotherapy: a preliminary study." BMC cancer 20.1 (2020): 1-9.
20. A. J. Chou, D. S. Geller, R. Gorlick, Therapy for osteosarcoma, Pediatric Drugs 10(2008) 315-327.
21. C. A. Arndt, W. M. Crist, Common musculoskeletal tumors of childhood and adolescence,New England Journal of Medicine 341 (1999) 342-352.
22. Luetke, A.; Meyers, P.A.; Lewis, I.; Juergens, H. Osteosarcoma treatment—Where do we stand? A state of the art review. Cancer Treat. Rev. **2014**, 40, 523–532. [CrossRef] [PubMed].
23. Koutsomplia, G.; Lambrou, G.I. Resistance mechanisms in the radiation therapy of osteosarcoma: A brief review. J. Res. Pract. Musculoskelet. Syst. **2020**, 4, 15–19. [CrossRef].
24. Abhilash Shukla, Atul Patel, Bone cancer detection from X-ray and MRI images through image segmentation techniques, Int. J. Recent Technol. Eng. 8 (6) (2020) 273–278.

25. Ashish Sharma, Dhirendra P. Yadav, Hitendra Garg, Mukesh Kumar, BhishamSharma, Deepika Koundal, Bone cancer detection using feature extraction based machine learning model, Hindawi, Comput. Math. Methods Med. (2021) 7433186.
26. Arunachalam, Harish Babu, et al. "Viable and necrotic tumor assessmentfrom whole slide images of osteosarcoma using machine-learning anddeep-learning models." PloS one 14.4 (2019): e0210706.
27. K. Simonyan, Zisserman. A., Very deep convolutional networks for large-scaleimage recognition, 2014, 1409.1556, http://dx.doi.org/10.48550/arXiv.1409.1556.
28. N. Wahab, A. Khan, Y. S. Lee, Transfer learning based deep cnn for segmentation anddetection of mitoses in breast cancer histopathological images, Microscopy 68 (2019)216-233.
29. Mishra, R.; Daescu, O.; Leavey, P.; Rakheja, D.; Sengupta, A. Convolutional neural network for histopathological analysis ofosteosarcoma. J. Comput. Biol. **2018**, 25, 313–325. [CrossRef]
30. K. Sujatha, S. Jayalakshmi, P. Sinthia, M. Malathi, K. Ramkumar,S.-Q. Cao, and K. Harikrishnan, "Screening and Identity the BoneCancer/Tumor using Image Processing," 2018 International Conferenceon Current Trends towards Converging Technologies (ICCTCT), 2018.
31. Takafumi, Osteosarcoma. Place of publication not identified:SPRINGER Verlag, JAPAN, 2018.
32. Baidya Kayal, Esha, et al. "Segmentation of osteosarcoma tumor usingdiffusion weighted MRI: a comparative study using nine segmentationalgorithms." Signal, Image and Video Processing 14.4 (2020): 727-735.
33. Ma, Jing, Minglu Li, and Yongqiang Zhao. "Segmentation of multimodalityosteosarcoma mri with vectorial fuzzy connectedness theory."International Conference on Fuzzy Systems and Knowledge Discovery. Springer, Berlin, Heidelberg, 2005.
34. Huang, Lin, et al. "MSFCN-multiple supervised fully convolutionalnetworks for the osteosarcoma segmentation of CT images." Computermethods and programs in biomedicine 143 (2017): 67-74.
35. P. P. Lin, S. Patel, Osteosarcoma, in: Bone Sarcoma, Springer, 2013, pp. 75-97.
36. J. C. Wittig, J. Bickels, D. Priebat, J. Jelinek, K. Kellar-Graney, B. Shmookler, M. M.Malawer, Osteosarcoma: a multidisciplinary approach to diagnosis and treatment,American family physician 65 (2002) 1123.
37. D. S. Geller, R. Gorlick, Osteosarcoma: a review of diagnosis, management, and treatmentstrategies, Clin Adv Hematol Oncol 8 (2010) 705-718.
38. A. Madabhushi, G. Lee, Image analysis and machine learning in digital pathology: Challengesand opportunities, Medical Image Analysis 33 (2016) 170 { 175. 20th anniversaryof the Medical Image Analysis journal (MedIA).
39. G. Litjens, C. I. S_anchez, N. Timofeeva, M. Hermsen, I. Nagtegaal, I. Kovacs,C. Hulsbergen-Van De Kaa, P. Bult, B. Van Ginneken, J. Van Der Laak, Deep learningas a tool for increased accuracy and e_ciency of histopathological diagnosis, Scienti_c reports 6 (2016) 26286.
40. C. Szegedy, W. Liu, Y. Jia, P. Sermanet, S. Reed, D. Anguelov, D. Erhan, V. Vanhoucke,A. Rabinovich, Going deeper with convolutions, in: Proceedings of the IEEE conferenceon computer vision and pattern recognition, 2015, pp. 1-9.
41. J. Chang, J. Yu, T. Han, H.-j. Chang, E. Park, A method for classifying medical imagesusing transfer learning: A pilot study on histopathology of breast cancer, in: 2017IEEE 19th International Conference on e-Health Networking, Applications and Services (Healthcom), IEEE, 2017, pp. 1-4.
42. M. Yanagawa, H. Niioka, A. Hata, N. Kikuchi, O. Honda, H. Kurakami, E. Morii,M. Noguchi, Y.Watanabe, J. Miyake, et al., Application of deep learning (3-dimensionalconvolutional neural

network) for the prediction of pathological invasiveness in lungadenocarcinoma: A preliminary study, Medicine 98 (2019).

43. C. Sun, A. Xu, D. Liu, Z. Xiong, F. Zhao, W. Ding, Deep learning-based classi_cation ofliver cancer histopathology images using only global labels, IEEE Journal of Biomedicaland Health Informatics 24 (2020) 1643-1651. doi:10.1109/JBHI.2019.2949837.
44. Y. Celik, M. Talo, O. Yildirim, M. Karabatak, U. R. Acharya, Automated invasiveductal carcinoma detection based using deep transfer learning with whole-slide images,Pattern Recognition Letters (2020).
45. H. B. Arunachalam, R. Mishra, O. Daescu, K. Cederberg, D. Rakheja, A. Sengupta,D. Leonard, R. Hallac, P. Leavey, Viable and necrotic tumor assessment from wholeslide images of osteosarcoma using machine-learning and deep-learning models, PloSone 14 (2019) e0210706.
46. Park, D.E.; Cheng, J.; Berrios, C.; Montero, J.; Cortes-Cros, M.; Ferretti, S.; Arora, R.; Tillgren, M.L.; Gokhale, P.C.; DeCaprio, J.A.Dual inhibition of mdm2 and mdm4 in virus-positive merkel cell carcinoma enhances the p53 response. Proc. Natl. Acad. Sci.USA **2019**, 116, 1027–1032. [CrossRef]
47. Vlahopoulos, S.A.; Cen, O.; Hengen, N.; Agan, J.; Moschovi, M.; Critselis, E.; Adamaki, M.; Bacopoulou, F.; Copland, J.A.;Boldogh, I.; et al. Dynamic aberrant nf-kappab spurs tumorigenesis: A new model encompassing the microenvironment. CytokineGrowth Factor Rev. **2015**, 26, 389–403. [CrossRef]
48. Nouri, M.; Massah, S.; Caradec, J.; Lubik, A.A.; Li, N.; Truong, S.; Lee, A.R.; Fazli, L.; Ramnarine, V.R.; Lovnicki, J.M.; et al.Transient sox9 expression facilitates resistance to androgen-targeted therapy in prostate cancer. Clin Cancer Res **2020**, 26, 1678–1689.[CrossRef] [PubMed]
49. Smeland, S.; Bielack, S.S.; Whelan, J.; Bernstein, M.; Hogendoorn, P.; Krailo, M.D.; Gorlick, R.; Janeway, K.A.; Ingleby, F.C.;Anninga, J.; et al. Survival and prognosis with osteosarcoma: Outcomes in more than 2000 patients in the euramos-1 (European and american osteosarcoma study) cohort. Eur. J. Cancer **2019**, 109, 36–50. [CrossRef] [PubMed]
50. Leavey, P.; Arunachalam, H.B.; Armaselu, B.; Sengupta, A.; Rakheja, D.; Skapek, S.; Cederberg, K.; Bach, J.-P.; Glick, S.; Ni'Suilleabhain, M. Implementation of Computer-Based Image Pattern Recognition Algorithms to Interpret Tumor Necrosis; A First Step inDevelopment of a Novel Biomarker in Osteosarcoma; Pediatric Blood & Cancer; Wiley: Hoboken, NJ, USA, 2017; p. S52.